Temperature Dependence of IP_3-Mediated Local and Global Ca^{2+} Signals

George D. Dickinson[†*] and Ian Parker[†‡]
[†]Department of Neurobiology and Behavior and [‡]Department of Physiology and Biophysics, University of California, Irvine, California

ABSTRACT We examined the effect of temperature (12–40°C) on local and global Ca^{2+} signals mediated by inositol trisphosphate receptor/channels (IP_3R) in human neuroblastoma (SH-SY5Y) cells. The amplitudes and spatial spread of local signals arising from single IP_3R (blips) and clusters of IP_3R (puffs) showed little temperature dependence, whereas their kinetics (durations and latencies) were markedly accelerated by increasing temperature. In contrast, the amplitude of global Ca^{2+} waves increased appreciably at lower temperatures, probably as a result of the longer duration of IP_3R channel opening. Several parameters, including puff and blip durations, puff latency and frequency, and frequency of repetitive Ca^{2+} waves, showed a biphasic temperature dependence on Arrhenius plots. In all cases the transition temperature occurred at ~25°C, possibly reflecting a phase transition in the lipids of the endoplasmic reticulum membrane. Although the IP_3-evoked Ca^{2+} signals were qualitatively similar at 25°C and 36°C, one should consider the temperature sensitivity of IP_3-mediated signal amplitudes when extrapolating from room temperature to physiological temperature. Conversely, further cooling may be advantageous to improve the optical resolution of channel gating kinetics.

INTRODUCTION

Cytosolic Ca^{2+} signals mediated by Ca^{2+} liberation from the endoplasmic reticulum (ER) through inositol trisphosphate receptor/channels (IP_3R) are organized as a hierarchy of events ranging from single-channel signals to global Ca^{2+} waves that engulf the whole cell (1–4). Blips arise from stochastic openings of individual IP_3Rs (5,6); local Ca^{2+} puffs are generated by the openings of several IP_3Rs within a cluster, orchestrated by the positive feedback of Ca^{2+} released by one channel promoting the opening of closely neighboring channels (7); and Ca^{2+} waves propagate by successive cycles of Ca^{2+} release, diffusion, and Ca^{2+}-induced Ca^{2+} release (CICR) from adjacent clusters (8,9).

We previously examined the temperature dependence of IP_3-mediated Ca^{2+} signaling by recording Ca^{2+}-activated Cl^- currents in *Xenopus* oocytes, and found that the frequency of repetitive Ca^{2+} oscillations slowed with cooling, and, surprisingly, that the amplitude of Ca^{2+}-evoked currents increased markedly with cooling (10). Since then, advances in imaging technology have made it possible to resolve cytosolic Ca^{2+} signals down to the level of individual channels, and thus we were interested in studying the temperature dependence of IP_3R properties at the single-channel and cluster levels in the intact cell, and determining how these properties affect global cellular signals. Here, we utilized total internal reflection fluorescence (TIRF) microscopy for high-resolution Ca^{2+} imaging in mammalian SH-SY5Y neuroblastoma cells (6), in conjunction with cytosolic loading with the slow Ca^{2+} buffer EGTA to inhibit cluster-cluster interactions and thus allow recording of autonomous local Ca^{2+} puffs and blips (11), or without EGTA to record global Ca^{2+} waves. Our principal finding is that Ca^{2+} permeation through the IP_3R channel shows little temperature dependence, but channel gating is markedly temperature dependent. The amplitudes of blips and puffs were little affected by temperature, and the mean number of channels contributing to puffs remained unchanged, but the durations of both blips and puffs shortened markedly with increasing temperature. The increased amplitude of global Ca^{2+} signals at lowered temperatures can thus be attributed to a prolongation of IP_3R channel openings, and not to an increased conductance of the individual channels.

MATERIALS AND METHODS

Cell culture and preparation of cells for imaging

Human neuroblastoma SH-SY5Y cells were cultured as previously described (6). Briefly, cells were incubated at 37°C in a humidified incubator (95% air, 5% CO_2) in a 1:1 mixture of Ham's F12 medium and Eagle's minimal essential medium, supplemented with fetal calf serum (10%, v/v) and nonessential amino acids (1%, v/v; all media were obtained from Invitrogen, Carlsbad, CA). The cells were passaged every 2–3 days and used for up to 20 passages. Cells were harvested 4 days before imaging in phosphate-buffered saline without Ca^{2+} or Mg^{2+}, and added to Petri dishes with glass coverslip bases (35 mm dish, No. 1.0 coverglass; MatTek, Ashland, MA) at a density of 3×10^4 cells/ml. Cells were loaded with membrane-permeant acetoxymethyl (AM) or propionyloxymethyl (PM) esters of fluo-4 and caged IP_3 (ci-IP_3) by incubation in Hepes-buffered saline (HBS, composition in mM: NaCl 135, KCl 5, $MgSO_4$ 1.2, $CaCl_2$ 2.5, Hepes 5, glucose 10, pH 7.4). Cells were first loaded in HBS containing ci-IP_3-PM (1 μM; SiChem, Bremen, Germany) at 21°C for 45 min, and then with ci-IP_3-PM (1 μM) and fluo-4-AM (5 μM) for 45 min before global calcium waves were imaged. Cells used for imaging of puffs and blips received an additional 45 min of incubation with HBS containing EGTA-AM (5 μM; Invitrogen). All cells were washed with HBS and allowed at least 30 min for desterification before imaging. AM and PM esters were made up in dimethyl sulfoxide containing 20% Pluronic F-127 (Invitrogen).

Submitted September 13, 2012, and accepted for publication December 13, 2012.

*Correspondence: dickinsg@uci.edu

Editor: Randall Rasmusson.

0006-3495/13/01/0386/10 $2.00

http://dx.doi.org/10.1016/j.bpj.2012.12.024

TIRF microscopy

Changes in intracellular Ca^{2+} concentration ($[Ca^{2+}]_i$) were imaged using an in-house-built TIRF microscope system constructed around an Olympus IX 70 microscope with a 60× TIRF objective (NA, 1.45) as previously described (6). Fluo-4 fluorescence was excited at 488 nm with an argon-ion laser, and images of emitted fluorescence ($\lambda > 510$ nm) were captured at a resolution of 128 × 128 pixels (1 pixel = 0.33 μm) at 500 frames s^{-1} using a Cascade 128 electron-multiplied ccd camera (Roper Scientific, Tucson, AZ). The excitation laser beam was focused centrally at the back aperture of the objective for wide-field excitation or to the extreme edge of the aperture for TIRF imaging.

Photolysis of ci-IP_3 was evoked by a flash of UV light (350–400 nm) from an arc lamp focused to uniformly illuminate a region slightly larger than the imaging frame. Uncaging of ci-IP_3 released i-IP_3, a metabolically stable isopropylidene analog of IP_3, which evoked puff activity that persisted for several minutes. The flash duration was varied to regulate the amount of iIP_3 released. Image data were acquired as stack files using MetaMorph (Universal Imaging/Molecular Devices, Sunnyvale, CA) and were stored for offline analysis.

Fluorescence signals are expressed as a ratio ($\Delta F/F_0$) of the mean change in fluorescence (ΔF) at each pixel, after stimulation at a given region of interest (ROI), relative to the resting fluorescence (F_0). To measure global changes in $[Ca^{2+}]_i$, the ROI was set to encompass the majority of the cytoplasm, excluding the nucleus. To measure the rate-of-rise of global responses, a 6 × 6 pixel (2 × 2 μm) ROI was located on the site of initiation of the signal. To monitor puff activity in EGTA-loaded cells, 3 × 3 pixel (1 × 1 μm) ROIs were centered on visually identified puff sites that were sufficiently isolated to avoid bleed-through from nearby sites. Fluorescence traces were measured as the average intensity within an ROI. Microcal Origin Version 6.0 (OriginLab, Northampton, MA) was used for analysis and graphing.

Ionomycin release of Ca^{2+} from intracellular stores

Evaluation of the Ca^{2+} content of SH-SY5Y intracellular stores was carried out on fluo-4-loaded cells. Cells were washed three times in Ca^{2+}-free HBS (composition in mM: EGTA 1, NaCl 135, KCl 5, $MgSO_4$ 1.2, Hepes 5, glucose 10, pH 7.4) before addition of ionomycin (1 μM; Invitrogen). Responses were compared between cells that were or were not previously incubated with thapsigargin (1 μM; Invitrogen) for 1 h in normal HBS.

Control of temperature

$[Ca^{2+}]_i$ signals were recorded at a variety of temperatures using an in-house-built brass 35 mm Petri dish holder incorporating two Peltier elements with water-circulating heat exchangers. The temperature of the medium in the dish could be cooled to as low as 12°C or warmed to 40°C, regulated by the magnitude and polarity of direct current passed through the Peltier elements. The temperature of the bathing solution immediately next to the cells was continuously monitored via a small thermocouple probe and digital thermometer (Type-K beaded probe; Fisher Scientific, Pittsburg, PA).

Experiments were performed in randomized temperature order. To examine the reversibility of responses after increases or decreases of temperature, we measured control responses at 21°C and then again at this temperature after cooling to 12°C or warming to 36°C for 15 min. No substantial differences were observed in the amplitude of global signals evoked by photorelease of i-IP_3 or in or the duration of puffs in EGTA-loaded cells. Compared with the mean responses obtained at 21°C, a 16.7% ± 13% decrease in the mean amplitudes of global signals was seen after heating (n = 23 cells) and a 18.9% ± 11.0% decrease was observed after cooling (n = 33 cells). For puff durations, a 17.9% ± 6.1% decrease was seen after heating (n = 21 cells) and a 14.1 ± 4.4% decrease was observed after cooling (n = 65 cells).

Basal free $[Ca^{2+}]_i$ measurements

The resting $[Ca^{2+}]_i$ of SH-SY5Y cells at 12°C, 22°C, and 36°C was assessed as follows: Plated cells were incubated in HBS containing fura-2-AM (2.5 μM; Invitrogen) for 45 min at 21°C. The cells were then washed into HBS (3 × 1 ml), allowed to deesterify for 30 min, and imaged using the InCyt Im2 Ratio Imaging System (Intracellular Imaging; Cincinnati, OH) fitted with a 40× Fluor oil objective (NA 1.30). Fura-2 fluorescence ($\lambda > 440$ nm) image pairs were recorded every 1.2 s with alternate excitation at 340 and 380 nm. $[Ca^{2+}]_i$ was estimated from ratiometric 340/380 nm images by comparison with a standard curve generated using a Fura-2 Calcium Imaging Calibration Kit (Invitrogen) after correction for temperature-dependent changes in the affinity of fura-2 as previously described (12).

Determination of temperature coefficients and transition points

To quantify the dependence of various Ca^{2+} wave and puff characteristics on temperature, we calculated the Q_{10} temperature coefficient for a 10°C change in temperature as follows:

$$Q_{10} = \left(\frac{R2}{R1}\right)^{\frac{10}{(T2-T1)}}$$

where R2 and R1 are the parameter values at temperatures T2 and T1, respectively. $Q_{10} > 1$ indicates an increase in parameter value with increasing temperature, $Q_{10} = 1$ indicates no temperature dependence, and $Q_{10} < 1$ indicates a decrease in parameter value with increasing temperature. Q_{10} values were determined from the slope of regression lines fitted to Arrhenius plots (logarithm of the measured parameter versus the reciprocal of absolute temperature). In several instances, we found differential sensitivities to temperature across the range explored, such that Arrhenius plots were better fit by two straight-line segments of different slopes, rather than by a single regression line. In these cases, segmental linear regression was performed using GraphPad Prism (version 6.0 for Windows; GraphPad Software, La Jolla, CA) to fit intersecting linear regressions. The transition point was not constrained and was a free parameter adjusted by the GraphPad software to obtain the optimal least-squares fit to the data.

Statistical analysis

Statistical significance was assessed in all cases by Student's t-test.

RESULTS

Temperature dependence of global IP_3-invoked Ca^{2+} signals in SH-SY5Y cells

We first examined global Ca^{2+} signals induced by flash photorelease of i-IP_3 in SH-SY5Y neuroblastoma cells that were not loaded with EGTA. Fig. 1 *A* shows representative images of fluo-4 Ca^{2+} fluorescence signals captured 15 s after UV flashes (160 ms duration) in cells at temperatures of 12°C, 22°C, and 36°C. Fig. 1 *B* shows individual whole-cell (excluding nucleus) fluorescence ratio measurements evoked by UV flashes of 20, 40, 80, 160, and

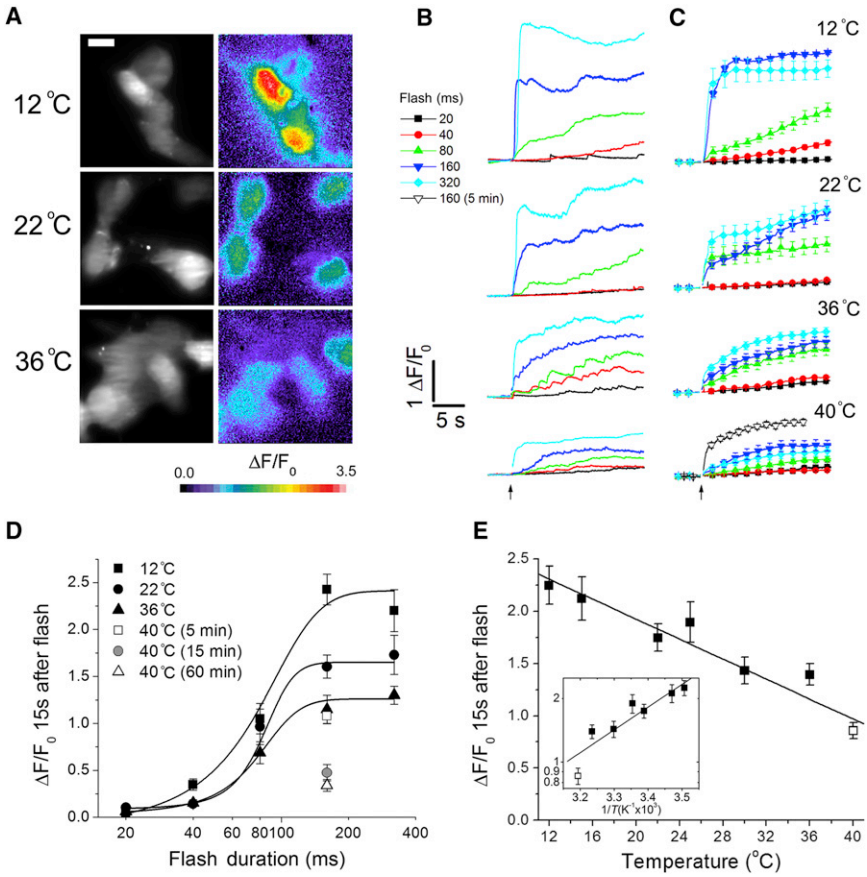

FIGURE 1 Temperature dependence of global Ca^{2+} signals. (*A*) Images of Ca^{2+} signals evoked by a 160 ms UV photolysis flash in SH-SY5Y cells at 12°C, 22°C, and 36°C. The grayscale images on the left show resting fluorescence to indicate the outlines of the cells. The color images on the right show single 15 ms exposures captured 15 s after the flash, depicting $\Delta F/F_0$ fluorescence ratios on a pseudo-color scale as indicated by the color bar, with warmer colors representing higher $[Ca^{2+}]_i$. (*B*) Representative fluorescence traces showing responses in cells evoked by photolysis flashes (*arrow*) of 20, 40, 80, 160, and 320 ms durations at temperatures of 12°C, 22°C, 36°C, and 40°C. Each trace shows the average fluorescence throughout the majority of a single cell, excluding the nucleus. Fluorescence is expressed as a ratio of fluorescence change (ΔF) relative to resting fluorescence (F_0) before stimulation. Cells were incubated at each temperature for ≥15 min before the flash. (*C*) Mean responses from ≥10 cells in response to different photolysis flash durations as indicated. The 40°C plot depicts mean responses from cells held at this temperature for ~5 min (*open symbols*) or 15 min (*solid symbols*) before recording. For the 5 min incubation at 40°C, only the response to the 160 ms flash is shown. (*D*) Plot of mean peak calcium signals ($\Delta F/F_0$) at different temperatures as a function of flash duration (logarithmic scale). Measurements were taken 15 s after the photolysis flash. The solid symbols plot the responses of cells that were maintained at the indicated temperatures for at least 15 min before the flash. The open symbols indicate the response of cells held at 40°C for 5 (*square*) or 60 min (*triangle*) before a 160 ms flash. Curves are fitted sigmoidal dose-response relationships. (*E*) Pooled data plotting the mean responses to 160 and 320 ms UV flashes as a function of temperature. The 40°C data (*open square*) were obtained ≤5 min after warming to this temperature. (n = 96, 53, 86, 42, 54, 103, and 86 cells at temperatures of 12°C, 15°C, 22°C, 26°C, 30°C, 36°C, and 40°C, respectively). In this and subsequent graphs, the main plot is shown on linear scales and the inset shows an Arrhenius plot of the same data with a logarithmic *y*-axis and temperature scaled as reciprocal kelvin. Data in the Arrhenius plot are fit by a single regression line corresponding to $Q_{10} = 0.73$. The line in the main graph is a regression fit. Error bars in all panels indicate mean ± 1 SE.

320 ms durations in cells held at temperatures of 12°C, 22°C, 36°C, and 40°C. The corresponding mean traces, each averaged from >10 cells, are shown in Fig. 1 *C*. Qualitatively, it is apparent that the maximal responses (attained ~15 s after photorelease) declined progressively with increasing temperature.

Two sets of data are shown in Fig. 1 *C* for the 160 ms flash at 40°C obtained ≤5 min after warming to this temperature (*open triangles*), and after holding at 40°C for 15 min (*solid triangles*). The responses to a 160 ms flash after warming to 40°C within 5 min were little different from those at 36°C (Fig. 1 *D*), whereas they reduced appreciably after holding at 40°C for 15 min (to 44% of the initial value). A further reduction was seen after holding at 40°C for 1 h (to 31% of the initial value). After the responses shown in Fig. 1 *D*, all further results achieved at 40°C were obtained within 5 min of reaching this temperature, to exclude the possibility of progressive damage to the cells while holding for long periods at this fever-level temperature.

We further analyzed the results in Fig. 1 *D* by separately plotting Ca^{2+} signals measured 15 s after photorelease of i-IP_3 as a function of flash duration at each temperature. The data were well fitted by sigmoid relationships, and the effect of increasing temperature was largely to scale down the amplitudes of the curves without an appreciable shift along the *x*-axis. The photolysis flash durations that gave a half-maximal fluorescence response were 73.8 ± 7.2, 82.5 ± 7.5 and 77.2 ± 6.8 ms at 12°C, 22°C, and 36°C, respectively. Given that response amplitudes appeared to reach a maximum for flash durations ≥ 160 ms, we pooled data from 160 and 320 ms flashes to examine the temperature dependence of the maximal global Ca^{2+} signal across a range of more closely spaced temperatures between 12°C and 40°C. Fig. 1 *E* shows this relationship, plotted both on linear scales and as an Arrhenius plot (*inset*). The data fitted well to a straight line over the entire temperature range, with a negative slope (i.e., reducing response at higher temperature) corresponding to a Q_{10} of 0.73.

Ca^{2+} wave velocity increases with increasing temperature

Global IP_3-invoked Ca^{2+} signals often began from a single location within the cell and subsequently propagated as a nondecremental wave (Fig. 2 *A*). To measure the wave velocity from the stack of raw fluorescence images, we placed a line across the cell, intersecting the point of origin of the wave (*horizontal line* in the first frame of Fig. 2 *A*), and created kymograph plots (Fig. 2 *B*) depicting the distance along the line (*x*-axis) versus time (*y*-axis, top to bottom). Kymograph images indicated that signals spread with markedly higher velocities at elevated temperatures (Fig. 2 *B*), and we quantified the wave velocities from the slopes of lines (*white lines* in Fig. 2 *B*) drawn along the foot of the wavefront. These data indicated a monotonic relation between increasing velocity with higher temperature (Fig. 2 *C*) corresponding to a Q_{10} of 1.56.

We assessed the rate-of-rise of the global signal by locating a 6 × 6 pixel ROI on the initiation site and measuring the slope ($\Delta F/F_0\ s^{-1}$) of a tangent fitted to the steepest part of the rising phase. Regression analysis (Fig. 2 *D*) revealed only a slight trend for the rate-of-rise to increase with temperature ($Q_{10} = 1.12$).

Most of the cells we examined (in the absence of EGTA) showed global Ca^{2+} responses to photoreleased i-IP_3 with time courses resembling those illustrated in Fig. 1 *B* (i.e., a fast initial rise followed by a sustained elevation). However, several cells displayed a pattern of strong oscillations superimposed on a more gradual elevation of baseline signal (*inset*, Fig. 2 *E*) similar to that previously reported for oscillatory SH-SY5Y cells at room temperature (13).

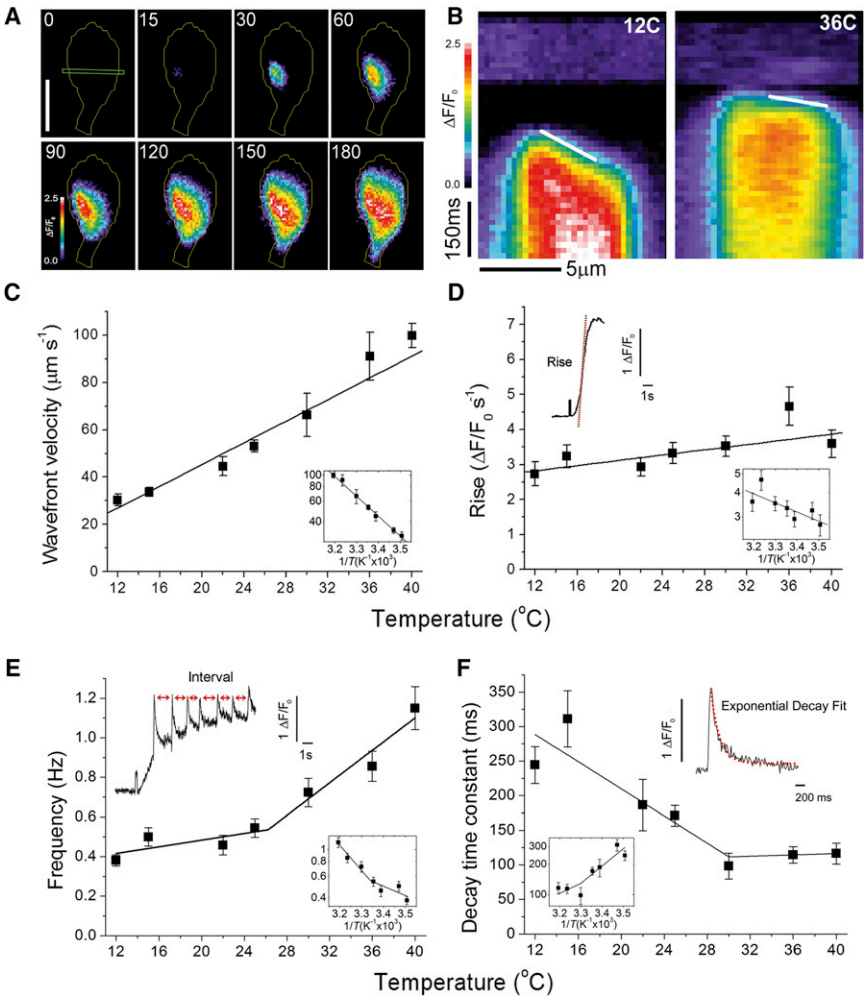

FIGURE 2 Ca^{2+} wave velocity, rate of rise, decay, and frequency are dependent on temperature. (*A*) Image sequence shows a Ca^{2+} wave spreading from a single point of origin in an SH-SY5Y cell at 12°C after a 160 ms UV flash. Each frame shows a single 15 ms exposure together with a superimposed outline of the cell periphery; acquisition times are indicated in milliseconds, beginning just before the start of the response and 255 ms after the photolysis flash. The images depict background-subtracted $\Delta F/F_0$ ratios, with the first frame showing a 10 μm scale bar, and the ROI used to generate the kymograph image in *B*. (*B*) Kymograph (linescan) images generated by measuring fluorescence ratio changes along 12 μm long lines positioned across cells, as illustrated in *A*, as a function of time. Data were obtained from representative cells at 12°C (*left*, the same cell as in *A*) and at 36°C (*right*). Time runs from top to bottom, with distance along the line depicted horizontally. Faint artifacts from the initiating UV flash are visible at the top of the image. White lines were superimposed by eye on the leading edge of the waves, and the slopes of these lines (distance/time) were used to calculate wavefront velocities. (*C*) Mean wavefront velocities estimated as in *B*, plotted as a function of temperature (n = 20, 15, 15, 15, 15, 15, and 25 cells at 12°C, 15°C, 22°C, 25°C, 30°C, 36°C, and 40°C, respectively). The lines fitted to the linear and Arrhenius plots correspond to a Q_{10} of ~1.56. (*D*) The rate-of-rise of global Ca^{2+} signals ($\Delta F/F_0\ s^{-1}$) was determined from fluorescence recordings from small (6 × 6 pixel; 2 × 2 μm) ROIs over the site of origin by measuring the slopes of tangents fitted to the rising phase of the signals, as illustrated in the inset. The plots show the rate-of-rise as a function of temperature between 12°C and 40°C ($n \geq 26$ cells for all temperatures). Lines are regression fits, with slopes corresponding to $Q_{10} = 1.12$. (*E*) The frequency of Ca^{2+} oscillations in 105 cells showing repetitive Ca^{2+} waves in response to 160 and 320 ms photolysis flashes was determined by measuring the intervals between successive waves, as illustrated in the inset showing a representative trace from a strongly oscillating cell at 22°C. The main graph and Arrhenius graph plot the mean Ca^{2+} spike frequency (1/mean interval) as a function of temperature (n = 15 cells at each temperature). Lines indicate segmental linear regression fits with transition points at 26.2°C. (*F*) The rate of decay of Ca^{2+} spikes was assessed in cells (n = 20) that demonstrated strong oscillatory responses. First-order exponential curves were fitted to the falling phase of the signals (illustrated by the *red curve* in the *inset*), and the resulting mean decay time constants are plotted as a function of temperature. The lines on the main and Arrhenius plots are segmental linear regression fits with transition points at 30.0°C.

A plot of mean oscillation frequency against temperature (Fig. 2 *E*) was best fit by two lines intersecting at a transition temperature of 26.2°C, with slopes corresponding to Q_{10} values of 1.24 between ~12°C and 26°C, and 1.67 for temperatures between ~26°C and 40°C.

We further measured the decay rate of fluorescence during the falling phase of individual spikes to determine the effect of temperature on the Ca^{2+} clearance rate from the cytosol (Fig. 2 *F*). Exponential fits to the falling phase of spikes indicate that the time constant decreased progressively between 12°C and 30°C (Q_{10} = 0.63), but little change was seen from 30°C to 40°C (Q_{10} = 0.96).

Temperature dependence of puff amplitudes

We next investigated the effects of temperature changes on Ca^{2+} puffs in cells that were loaded with the slow Ca^{2+} buffer EGTA (300 μM) to balkanize Ca^{2+} waves into autonomous local signals by inhibiting CICR between clusters of IP_3Rs (11,13). Fig. 3, *A* and *B*, show representative fluorescence records of puffs evoked by photoreleased i-IP_3 at 12°C, 22°C, and 36°C. The puffs had similar amplitudes at all temperatures; however, their durations were dramatically prolonged at cooler temperatures, and the latency from the UV flash to the first puff at a given site lengthened.

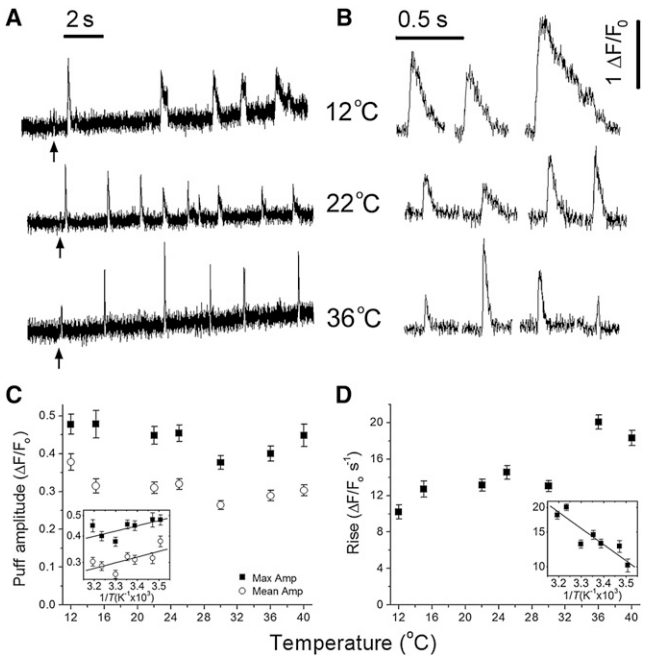

FIGURE 3 Local Ca^{2+} puff amplitudes display little temperature dependence. (*A*) Traces show representative records of Ca^{2+} puffs evoked at 12°C, 22°C, and 36°C by 160 ms UV photolysis flashes (*arrows*) in SH-SY5Y cells loaded with EGTA. Fluorescence was measured from 3 × 3 pixel (1 × 1 μm) ROIs centered on visually identified puff sites. (*B*) Selected examples of puffs at 12°C, 22°C, and 36°C shown on an expanded timescale. (*C*) Mean peak puff amplitudes plotted as a function of temperature. Open symbols are the mean of all puffs observed at each temperature (number of events = 200, 546, 880, 657, 866, 1034, and 721 at 12°C, 15°C, 22°C, 25°C, 30°C, 36°C, and 40°C, respectively). Solid symbols plot the means of the largest puff observed at each given site (number of sites = 43, 79, 123, 97, 107, 130, and 82, respectively). (*D*) Temperature dependence of the rate-of-rise of Ca^{2+} signals during puffs, measured from baseline to peak. The line in the inset Arrhenius plot is a linear regression fit.

Fig. 3 *C* shows measurements of both the mean amplitudes of all puffs observed at a given temperature (*open symbols*), and the means of the largest puff observed at each given site (*solid symbols*). Slopes of lines fitted to the Arrhenius plots correspond to a Q_{10} value of 0.94 for both. The mean rate-of-rise of the puffs showed a slightly higher temperature dependence, increasing progressively from 12°C to 40°C, and an Arrhenius plot showed a single component corresponding to a Q_{10} of 1.15 (Fig. 3 *D*).

Temperature dependence of ER Ca^{2+} store loading and basal cytosolic free $[Ca^{2+}]_i$

The magnitude of IP_3-evoked cytosolic Ca^{2+} signals is a function of Ca^{2+} concentrations within the ER and the cytosol, and also depends on the properties of the IP_3R channel. To examine whether temperature affects the amount of Ca^{2+} sequestered by SH-SY5Y cells, we used 1 μM ionomycin to mobilize Ca^{2+} from intracellular stores of fluo-4 loaded cells bathed in Ca^{2+}-free extracellular solution, and monitored the change in cytosolic $[Ca^{2+}]_i$ by wide-field epifluorescence imaging (Fig. 4 *A*). We obtained paired measurements from cells that preincubated with thapsigargin (1 μM; *solid symbols*) to inhibit SERCA activity and thereby deplete ER Ca^{2+} stores, or not preincubated (*open symbols*). The difference between these measurements thus provides a specific measure of SERCA-dependent ER Ca^{2+} store filling (Fig. 4 *B*). No appreciable changes in ER Ca^{2+} content were apparent at temperatures of 12°C, 22°C, and 36°C.

Our measurements of Ca^{2+}-dependent fluo-4 fluorescence signals are presented as ratios of fluorescence increases after photorelease of i-IP_3 (ΔF) divided by the initial resting fluorescence before stimulation (F_o). Thus, temperature-dependent changes in the ratio signal $\Delta F/F_0$ evoked by a constant stimulus could reflect changes in basal cytosolic $[Ca^{2+}]_i$ as well as changes in Ca^{2+} liberation. We therefore made fura-2 ratiometric measurements of basal $[Ca^{2+}]_i$ at temperatures of 12–36°C. Whereas the F_{340}/F_{380} ratio tended to increase with increasing temperature (*gray bars*, Fig. 4 *C*), corresponding estimates of basal $[Ca^{2+}]_I$, after correcting for temperature-dependent changes in affinity of fura-2 (12), indicated that basal $[Ca^{2+}]_i$ is substantially independent of temperature (*black bars*, Fig. 4 *C*).

Temperature dependence of puff kinetics

As is evident in Fig. 3 *A*, increasing temperatures produced much greater changes in the kinetics of local Ca^{2+} puffs

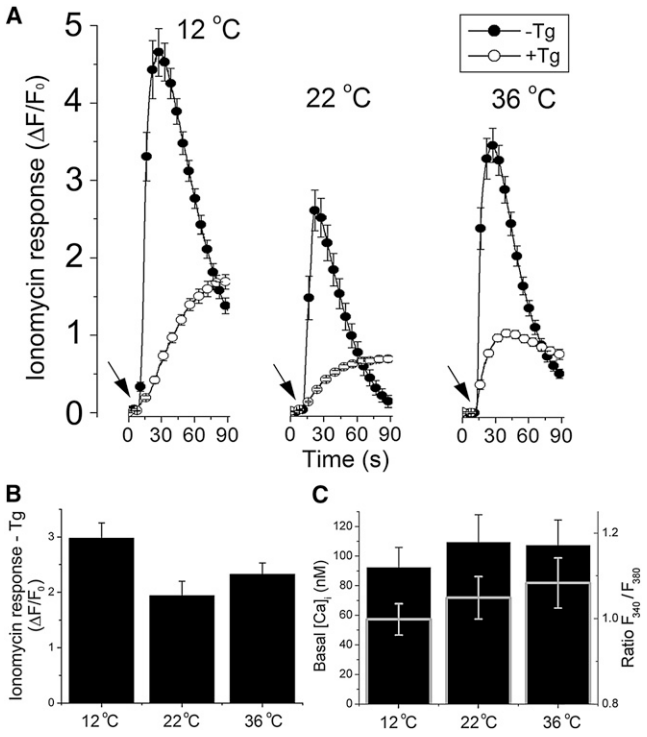

FIGURE 4 Temperature dependence of Ca^{2+} store filling and basal $[Ca^{2+}]_i$. (*A*) Solid circles show mean whole-cell fluorescence signals recorded from SH-SY5Y cells after bath addition of 1 μM ionomycin (indicated by *arrows*) in solution containing no added Ca^{2+} and 1 mM EGTA at 12°C, 22°C, and 36°C (n = 66, 65, and 80 cells, respectively). The mean responses to the same treatment in cells that were incubated with 1 μM thapsigargin for 1 h before recording are shown by open circles (n = 26, 45, and 20 cells, respectively). (*B*) Bars indicate the mean thapsigargin-sensitive response to ionomycin in the cells in panel *A*. A Student's *t*-test indicated no significant difference between responses at 36°C and either 12°C or 22°C (*C*) Measurements of mean basal $[Ca^{2+}]_i$ derived from ratiometric fura-2 recordings in SH-SY5Y cells incubated at 12°C, 22°C, and 36°C (n = 5 replicate experiments, with $\geq$25 cells per experiment) for 15 min (*black bars*). The raw F_{340}/F_{380} ratios used to derive basal $[Ca^{2+}]_i$ are superimposed in light gray. Corresponding estimates of basal $[Ca^{2+}]_i$ were determined by comparison with in vitro calibration of fura-2 ratios at 22°C after correcting for temperature-dependent changes in K_d (325, 275, and 224 nM at 12°C, 22°C, and 36°C, respectively (12)). A Student's *t*-test indicated no significant differences between responses at any of the temperatures examined.

than in their amplitudes. Fig. 5 *A* plots the distributions of puff durations (measured at half-maximum amplitude), depicting a shift toward shorter events as the temperature was raised from 12°C to 22°C and 36°C, and mean puff durations are plotted as a function of temperature in Fig. 5 *B*. Over the range from 12°C to 40°C, the puff duration shortened with a Q_{10} of ~0.49, and an Arrhenius plot (*inset*, Fig. 5 *B*) showed a hint of a transition point at ~25°C.

Puff latencies (i.e., the time from photorelease of i-IP_3 to the occurrence of the first puff at a given site) also shortened markedly with temperature. Fig. 5 *C* plots the spread of puff latencies (*vertical lines*) and the mean latency for all puff sites (*open circles*) at 12°C, 22°C, and 36°C. It is apparent that the spread of latencies narrowed and the mean latency shortened at warmer temperatures. Fig. 5 *D* further plots the mean puff latencies as functions of temperature between 12°C and 40°C, as measured from the arithmetic mean of observations at each temperature and derived from exponential fits to the distributions of latencies. Both sets of data show a similar relationship, with puff latency shortening from 7–11 s at 12°C to ~2 s at 40°C. An Arrhenius plot (Fig. 5 *D*, *inset*) was best fit by two segments, intersecting at 25°C, and with slopes corresponding to a Q_{10} of 0.38 at lower temperatures and 0.73 at higher temperatures.

The mean frequency of puffs evoked by a constant photolysis flash increased by only ~50% upon warming from 12°C to 40°C (Fig. 5 *E*), but an Arrhenius plot revealed a two-component relationship, with almost no temperature dependence below ~24°C (Q_{10} = 1.01) and a stronger dependence (Q_{10} = 1.32) above this temperature (Fig. 5 *E*, *inset*).

Temperature dependence of single IP_3R channels

Ca^{2+} puffs in SH-SY5Y cells involve the synchronous opening of several (mean ~6) tightly clustered IP_3R channels (6). TIRF imaging in EGTA-loaded cells can further resolve smaller signals (blips) originating at sites that apparently contain only a single functional receptor (6), enabling analysis of the temperature dependence of single-channel conductance and gating properties.

Fig. 6 *A* shows representative examples of recordings from blip sites at temperatures of 12°C, 22°C, and 36°C, and Fig. 6 *B* plots as functions of temperature both the arithmetic means of the blip durations and the time constants (τ) derived from single exponential fits to the distributions of blip durations, measured at each temperature. Measurements of τ are likely to provide a more accurate estimate of the mean duration of blips, as the arithmetic mean will be skewed high by failure to resolve brief openings in the face of background noise and limited recording bandwidth (6). From Fig. 6 *B* it is apparent that the arithmetic means are indeed significantly higher than the corresponding values of τ derived from exponential fits. Nevertheless, both sets of data show a similar temperature dependence, with the mean blip durations (single-channel open times) shortening ~3.1- to 3.4-fold from 12°C to 40°C. An Arrhenius plot of blip durations (τ) indicates that the data are best fit by two lines, with a transition point at ~25°C (Fig. 6 *B*, *inset*), and a steep temperature dependence (Q_{10} = 0.38) from 12°C to 25°C but little or no temperature dependence above 25°C (Q_{10} = 0.95).

Our estimates of mean blip duration (τ) at 22°C and 25°C (22.9 ± 1.8 and 15.5 ± 4.5 ms, respectively) are in good agreement with the value of 17 ms previously observed at room temperature (6), and with the mean open dwell time of 13.5 ms for IP_3R observed during patch clamp of

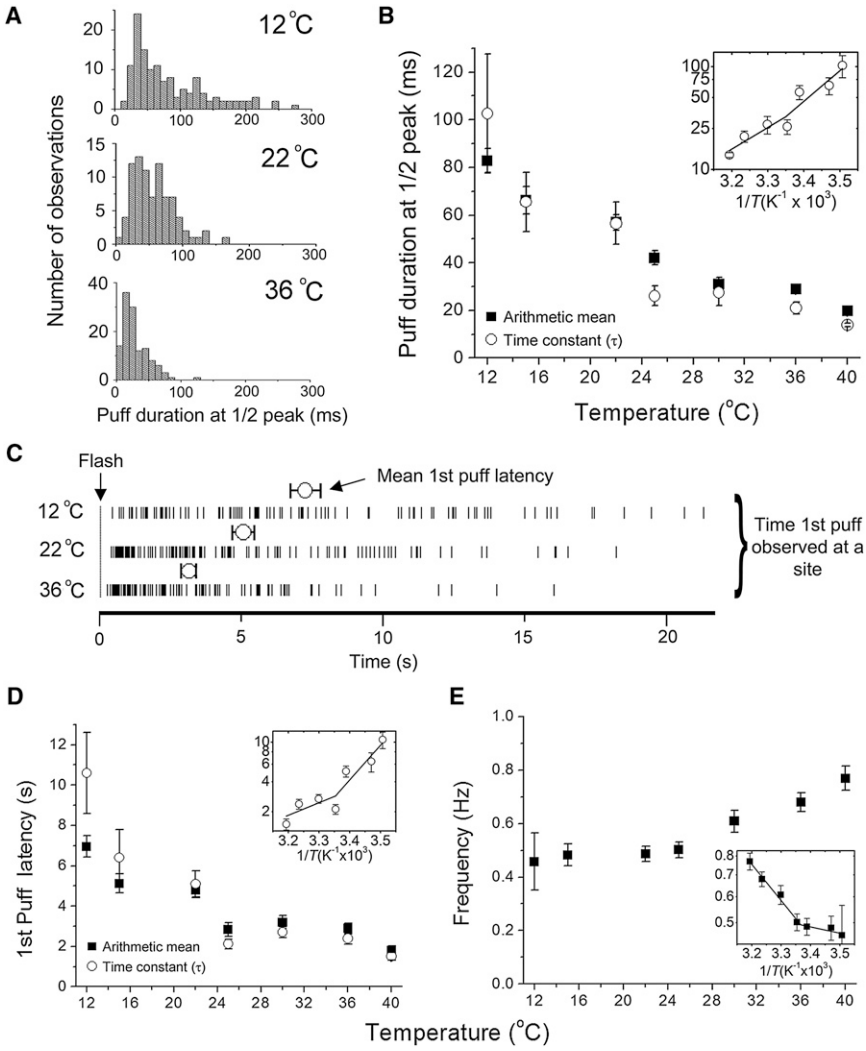

FIGURE 5 Dependence of puff kinetics on temperature. (*A*) Distributions of puff durations (full duration at half-peak amplitude (FDHM)) at temperatures of 12°C, 22°C, and 36°C. Data are from 133, 85, and 124 events, respectively. (*B*) Mean puff durations (FDHM) as a function of temperature. Data points on the main graph show arithmetic means (*solid squares*) and mean values estimated from the time constant of exponential fits to distributions like those in *A* (*open circles*). The Arrhenius plot shows only the time constant data, and is fitted by segmental linear regression (transition point at 25.3°C). (*C*) Distributions of first puff latencies (time from end of the photolysis flash to the initial puff observed at a given site) at temperatures of 12°C, 22°C, and 36°C. Vertical dashes mark the timing of individual events, and open circles show mean values ± 1 SEM. Data are from >79 events at each temperature. (*D*) Plots of mean puff latencies as a function of temperature, showing both arithmetic mean values (*solid squares*) and values derived from exponential fits to distributions of latencies (*open circles*). The Arrhenius plot shows only the time constant data and is fitted by segmental linear regression (transition point at 25.0°C). (*E*) Plot of mean puff frequencies as a function of temperature. Data are from >70 puff sites at each temperature. The Arrhenius plot is fit by segmental linear regression (transition point at 23.9°C).

SH-SY5Y cell nuclei (J.K. Foskett and D. Mak, University of Pennsylvania, personal communication, 2009).

Single-channel Ca^{2+} flux is almost unaffected by temperature

The falling phase of puffs resembles a descending staircase, with discrete steps reflecting the closings of individual IP_3R channels (6). These steps were more readily apparent at low temperatures, where the puffs decayed more slowly, but could still be identified even at 36°C (Fig. 6 *C*). Distributions of dwell-state amplitudes during puffs (measured as $\Delta F/F_0$ from the step level to baseline) showed multiple peaks corresponding to the simultaneous opening of n = 1, 2, 3, etc. channels. As described previously (6,14), these peaks could be fitted by the sum of multiple Gaussian components (Fig. 6 *C*). Here, we used this method of analysis to determine whether the Ca^{2+} flux through individual IP_3R channels shows an appreciable temperature dependence. This would be difficult to measure from blip amplitudes alone, given the small amplitude of these signals in relation to background noise, but can be more accurately determined by comparing dwell-state amplitude levels at steps where a known number of channels are simultaneously open.

We obtained the distributions of dwell-state amplitudes during puffs at temperatures of 12°C, 22°C, and 36°C, and fitted these by the sums of multiple Gaussian curves with free parameters for the center value, standard deviation (SD), and area of each individual Gaussian (Fig. 6 *C*). Fig. 6 *D* shows a plot of the center values of the Gaussians against the ordinate number of that Gaussian (i.e., the mean fluorescence ratio signals ($\Delta F/F_0$) observed when a given number (n) of channels were open). We were able to obtain reliable estimates for values of n between 1 and 5, and over this range the data followed a linear relationship, confirming our previous finding that fluorescence signals from individual channels summate linearly during puffs (6,14). Importantly, the data obtained at 12°C, 22°C, and 36°C lie closely on the same line (Fig. 6 *D*), indicating that the single-channel fluorescence signal was almost independent of temperature over this range.

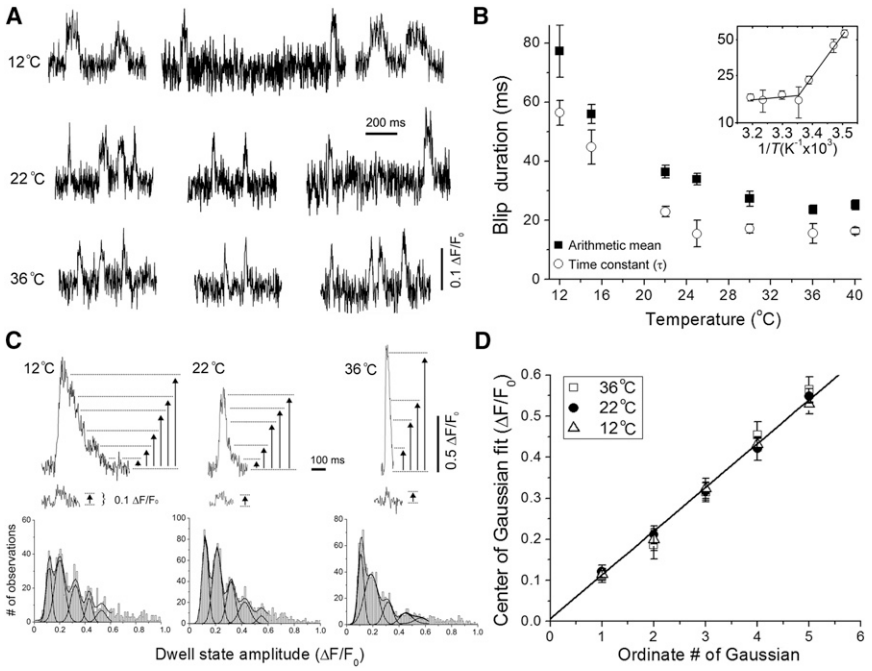

FIGURE 6 Temperature dependence of single-channel Ca^{2+} signals. (*A*) Representative fluorescence traces recorded at nine sites showing single-channel IP_3R signals (blips), at temperatures of 12°C, 22°C, and 36°C. (*B*) Plots of mean blip durations, derived as arithmetic means (*solid squares*) and from exponential fits to distributions (*open circles*), as functions of temperature. The Arrhenius plot is fitted by segmental linear regression (transition point at 25.1°C). (*C*) Inset traces illustrate dwell-state levels visually identified on the stepwise falling phase of puffs (*upper*), and single-channel blips (*lower*) at temperatures of 12°C, 22°C, and 36°C. The histograms show the corresponding distributions of dwell-state amplitude levels during puffs. The data (>1230 measurements at each temperature) are fit by sums of multiple Gaussian functions, as shown by smooth curves. (*D*) Plot of center values of the Gaussian fits as a function of the ordinate number of each Gaussian (i.e., the first, second, third, etc. Gaussian, in ascending order). Points show measurements at temperatures of 12°C (*open triangles*), 22°C (*solid circles*), and 36°C (*open squares*). Error bars: mean ± 1 SE of the Gaussian fits. The line is a regression fit to the entire data set.

DISCUSSION

Recent advances in fluorescence imaging techniques have made it possible to record local subcellular Ca^{2+} signals with a resolution at the single-channel level (15). Here, we used this approach to study the temperature dependence of the permeation and kinetic properties of IP_3 receptor/channels within intact human neuroblastoma cells, and to relate effects observed at the single-channel level to global Ca^{2+} signals.

First, however, we need to consider how interpretation of the effects of temperature on cytosolic Ca^{2+} signals is complicated by possible temperature-dependent changes in the properties of the fluorescent indicator dyes used to measure these signals. The dissociation constant of BAPTA and BAPTA-based probes decreases in vitro with increasing temperature (12), and this effect may be further compounded in vivo by interaction of the probes with cytosolic proteins. Moreover, the probe fluorescence itself is affected by temperature, regardless of the binding characteristics (although this effect was reported to be slight (<5%) for calcium green, a BAPTA-based probe closely related to fluo-4 (16)). Because we express fluo-4 signals (ΔF) as a pseudo-ratio relative to the basal fluorescence before stimulation (F_0), errors in measurements of Ca^{2+} transients arising from temperature-dependent changes in either property of the indicator should substantially cancel out. Specifically, the Ca^{2+}-bound and Ca^{2+}-free forms of indicators show approximately equivalent changes in fluorescence brightness with temperature (16), so we can control this temperature effect largely by taking the $\Delta F/F_0$ ratio. Similarly, temperature-dependent changes in indicator affinity are expected to result in approximately proportionate changes in ΔF and F_0 for small values of ΔF within the linear range of the indicator, given that the Ca^{2+}-independent fluorescence of fluo-4 is very low. Although this would not hold for the larger global signals ($\Delta F/F_0$ ~3) seen at low temperature, which approached the saturation point of the indicator ($\Delta F_{max}/F_0 > 6$, measured by ionomycin application in Ca^{2+}containing medium), the effect would be to underestimate the response magnitude, because increasing the affinity of fluo-4 at low temperature would increase F_0 while having no effect on F_{max}. Thus, the true increase in global Ca^{2+} signals at low temperature is probably even greater than indicated by our $\Delta F/F_0$ measurements, both because ΔF approached saturation and because F_0 increased. A remaining concern is whether cytosolic free $[Ca^{2+}]_i$ changes with temperature, which would affect measurements of F_0. Our fura-2 measurements indicate that resting $[Ca^{2+}]_i$ changed by no more than 29% between temperatures of 12°C, 22°C, and 36°C, consistent with previous findings in avian exocrine cells (12). Finally, we note that our conclusions largely concern the relationships between single-channel, cluster-level, and global Ca^{2+} signals, which, unlike measurements of absolute Ca^{2+} levels, will be unaffected by temperature-dependent changes in indicator properties because we are effectively taking a ratio of different types of signals evoked at each given temperature.

We interpret local Ca^{2+} fluorescence signals imaged by TIRF microscopy in EGTA-loaded cells as providing a good approximation of instantaneous Ca^{2+} flux into the

cytoplasm, that is to say, the fluorescence amplitude closely reflects instantaneous Ca^{2+} flux (Ca^{2+} current), and the time course tracks, within a few milliseconds, the opening and closing of Ca^{2+}-permeable channels (6). In the case of Ca^{2+} puffs, which reflect the concerted opening of several tightly clustered IP_3R channels, we found little effect of temperature on their mean peak amplitude. Furthermore, a quantal dissection of the steps during the falling phase of puffs, which reflect the closings of individual channels, revealed that the amplitude of unitary, single IP_3R channel signals was also essentially independent of temperature. We thus conclude that Ca^{2+} permeation through open IP_3R channels shows little or no temperature dependence, and that the average number of channels open at the peak of a puff remains roughly constant between 12°C and 40°C.

In marked contrast to the lack of temperature dependence of local IP_3-mediated Ca^{2+} signals, the amplitude of global, cell-wide signals increased appreciably with decreasing temperature ($Q_{10} = 0.73$). This cannot be attributed to any change in the apparent affinity of the IP_3R for IP_3, because the sigmoid dose-response relationships of global signals as a function of amount of photoreleased IP_3 showed no shift along the *x*-axis with temperature. Instead, the discrepancy between the temperature dependence of local versus global Ca^{2+} signals may be explained by the fact that the latter reflect the accumulation in the cytosol of Ca^{2+} ions liberated over several seconds. Puffs and blips are prolonged at lower temperatures, pointing to a prolongation of the mean open time of IP_3R channels. Thus, the efflux of Ca^{2+} that accumulates during global responses is expected to increase with cooling, even in the absence of any change in single-channel Ca^{2+} flux (Ca^{2+} current) or in the mean number of open channels.

Among the kinetic Ca^{2+} signaling parameters we measured, all of those that showed a strong temperature dependence displayed two-component Arrhenius plots with closely similar break-point temperatures (global wave frequency, 26.2°C; puff latency, 25.0°C; puff frequency, 23.9°C; puff duration, 25.3°C; and blip duration, 25.1°C). This behavior, as well as the transition temperature near 25°C, matches that reported for the temperature dependence of time-to-peak of Ca^{2+} sparks in rat cardiomyocytes, a measure of the open time of ryanodine receptor (RyR) channels (17). The discontinuous temperature dependence in Arrhenius plots is widely attributed to a phase transition of membrane lipids, which alters the apparent activation energy associated with the conformational change of opening of membrane ion channels (18). Thus, the ER membrane in SH-SY5Y cells likely undergoes a phase transition at ~25°C, resulting in a change in gating properties of the IP_3R.

Ca^{2+} wave propagation is considered as a reaction/diffusion system involving successive cycles of Ca^{2+} release from IP_3R clusters and diffusion to neighboring clusters to trigger CICR (8). We found that the velocity of global Ca^{2+} waves increased monotonically with increasing temperature, after a Q_{10} of ~1.56 between 12°C and 40°C, a value a little smaller than that reported for diffusion of $^{45}Ca^{2+}$ in cytosolic extracts ($Q_{10} = 2.04 \pm 0.36$ between 5°C and 25°C) (19). Thus, in agreement with similar findings for Ca^{2+} waves in *Xenopus* oocytes (20), it appears that diffusion, rather than Ca^{2+} activation of IP_3R channels, is the main rate-limiting factor in determining wave velocity in mammalian cells. This conclusion is further supported by our finding that the rate of rise of Ca^{2+} puffs (reflecting CICR-mediated recruitment of tightly spaced IP_3Rs, where diffusional delays would be negligible) is only modestly temperature dependent, with a Q_{10} of 1.12.

Two previous studies (17,21) examined the temperature dependence of Ca^{2+} sparks (elementary Ca^{2+} signals analogous to puffs that arise through concerted openings of clustered RyR channels) in cardiomyocytes. Ferrier et al. (21) reported that increasing the temperature from 22°C to 37°C reduced the incidence, frequency, amplitudes, and time-to-peak of sparks, but had little effect on their spatial width or decay times. On the other hand, Fu et al. (17) looked over a greater range of temperatures (10–35°C) with a larger dataset and reported that, in similarity to our findings on the temperature dependence of puffs, the amplitude and spatial width of sparks were insensitive to changes in temperature, whereas their frequency, time-to-peak, and decay times were all accelerated at higher temperatures.

As a matter of practical convenience, we (6) and other groups (22–24) generally image Ca^{2+} signals in mammalian cell lines at room temperature instead of the more physiologically appropriate 37°C. Our results show that the use of this lower temperature substantially enhances the amplitude and decreases the frequency of global IP_3-mediated Ca^{2+} signals, which accords with results obtained in diverse other cell types. For example, rapid cooling evokes large oscillatory Ca^{2+}-activated Cl^- currents in *Xenopus* oocytes when the IP_3 pathway is activated (10), and is reported to increase the amplitudes of IP_3-mediated Ca^{2+} signals in various cultured glial cells, including Schwann cells and olfactory ensheathing cells (25), and astrocytes (26). Thus, the temperature sensitivity of the CICR underlying global IP_3-mediated signals appears to be a general phenomenon, and we need to consider this when extrapolating results obtained at room temperature to body temperature.

In terms of local Ca^{2+} signals, the predominant effect of reduced temperature is to slow the kinetics of IP_3R channel gating while having little effect on the permeation properties. Indeed, further cooling may be experimentally advantageous to improve the resolution of single-channel events. The mean lifetime of single IP_3R channel openings (blips) and the durations of stepwise transitions during the falling phase of puffs as individual channels close are on the order of 10–20 ms at room temperature. This timescale is not much longer than the kinetic resolution of optical single-channel Ca^{2+} imaging (typically a few milliseconds), as

determined by the frame rate of currently available cameras, the decay kinetics of the local Ca^{2+} signal (27), and the need for a sufficiently long exposure time to achieve an acceptable signal/noise ratio. By cooling from 24°C to 12°C, it is possible to prolong single-channel signals ~3-fold without appreciably reducing their amplitude.

This work was supported by grants from the National Institutes of Health (GM048071 and GM065830).

REFERENCES

1. Parker, I., J. Choi, and Y. Yao. 1996. Elementary events of $InsP_3$-induced Ca^{2+} liberation in *Xenopus* oocytes: hot spots, puffs and blips. *Cell Calcium.* 20:105–121.
2. Bootman, M. D., M. J. Berridge, and P. Lipp. 1997. Cooking with calcium: the recipes for composing global signals from elementary events. *Cell.* 91:367–373.
3. Berridge, M. J. 1997. Elementary and global aspects of calcium signalling. *J. Physiol.* 499:291–306.
4. Berridge, M. J., P. Lipp, and M. D. Bootman. 2000. The versatility and universality of calcium signalling. *Nat. Rev. Mol. Cell Biol.* 1:11–21.
5. Parker, I., and Y. Yao. 1996. Ca^{2+} transients associated with openings of inositol trisphosphate-gated channels in *Xenopus* oocytes. *J. Physiol.* 491:663–668.
6. Smith, I. F., and I. Parker. 2009. Imaging the quantal substructure of single IP_3R channel activity during Ca^{2+} puffs in intact mammalian cells. *Proc. Natl. Acad. Sci. USA.* 106:6404–6409.
7. Yao, Y., J. Choi, and I. Parker. 1995. Quantal puffs of intracellular Ca^{2+} evoked by inositol trisphosphate in *Xenopus* oocytes. *J. Physiol.* 482:533–553.
8. Callamaras, N., J. S. Marchant, …, I. Parker. 1998. Activation and coordination of $InsP_3$-mediated elementary Ca^{2+} events during global Ca^{2+} signals in *Xenopus* oocytes. *J. Physiol.* 509:81–91.
9. Smith, I. F., S. M. Wiltgen, …, I. Parker. 2009. Ca(2+) puffs originate from preestablished stable clusters of inositol trisphosphate receptors. *Sci. Signal.* 2:ra77.
10. Miledi, R., I. Parker, and K. Sumikawa. 1987. Oscillatory chloride current evoked by temperature jumps during muscarinic and serotonergic activation in *Xenopus* oocyte. *J. Physiol.* 383:213–229.
11. Dargan, S. L., and I. Parker. 2003. Buffer kinetics shape the spatiotemporal patterns of IP_3-evoked Ca^{2+} signals. *J. Physiol.* 553:775–788.
12. Shuttleworth, T. J., and J. L. Thompson. 1991. Effect of temperature on receptor-activated changes in $[Ca^{2+}]_i$ and their determination using fluorescent probes. *J. Biol. Chem.* 266:1410–1414.
13. Smith, I. F., S. M. Wiltgen, and I. Parker. 2009. Localization of puff sites adjacent to the plasma membrane: functional and spatial characterization of Ca^{2+} signaling in SH-SY5Y cells utilizing membrane-permeant caged IP_3. *Cell Calcium.* 45:65–76.
14. Dickinson, G. D., D. Swaminathan, and I. Parker. 2012. The probability of triggering calcium puffs is linearly related to the number of inositol trisphosphate receptors in a cluster. *Biophys. J.* 102:1826–1836.
15. Parker, I., and I. F. Smith. 2010. Recording single-channel activity of inositol trisphosphate receptors in intact cells with a microscope, not a patch clamp. *J. Gen. Physiol.* 136:119–127.
16. Oliver, A. E., G. A. Baker, …, J. H. Crowe. 2000. Effects of temperature on calcium-sensitive fluorescent probes. *Biophys. J.* 78:2116–2126.
17. Fu, Y., G. Q. Zhang, …, S. Q. Wang. 2005. Temperature dependence and thermodynamic properties of Ca^{2+} sparks in rat cardiomyocytes. *Biophys. J.* 89:2533–2541.
18. Seeger, H. M., L. Aldrovandi, …, P. Facci. 2010. Changes in single K(+) channel behavior induced by a lipid phase transition. *Biophys. J.* 99:3675–3683.
19. Sidell, B. D., and J. R. Hazel. 1987. Temperature affects the diffusion of small molecules through cytosol of fish muscle. *J. Exp. Biol.* 129:191–203.
20. Lechleiter, J. D., and D. E. Clapham. 1992. Molecular mechanisms of intracellular calcium excitability in *X. laevis* oocytes. *Cell.* 69:283–294.
21. Ferrier, G. R., R. H. Smith, and S. E. Howlett. 2003. Calcium sparks in mouse ventricular myocytes at physiological temperature. *Am. J. Physiol. Heart Circ. Physiol.* 285:H1495–H1505.
22. Bootman, M., E. Niggli, …, P. Lipp. 1997. Imaging the hierarchical Ca^{2+} signalling system in HeLa cells. *J. Physiol.* 499:307–314.
23. Palmer, A. E., and R. Y. Tsien. 2006. Measuring calcium signaling using genetically targetable fluorescent indicators. *Nat. Protoc.* 1: 1057–1065.
24. Guatimosim, S., C. Guatimosim, and L. S. Song. 2011. Imaging calcium sparks in cardiac myocytes. *Methods Mol. Biol.* 689:205–214.
25. Stavermann, M., K. Buddrus, …, C. Lohr. 2012. Temperature-dependent calcium-induced calcium release via $InsP_3$ receptors in mouse olfactory ensheathing glial cells. *Cell Calcium.* 52:113–123.
26. Schipke, C. G., A. Heidemann, …, H. Kettenmann. 2008. Temperature and nitric oxide control spontaneous calcium transients in astrocytes. *Cell Calcium.* 43:285–295.
27. Shuai, J., and I. Parker. 2005. Optical single-channel recording by imaging Ca^{2+} flux through individual ion channels: theoretical considerations and limits to resolution. *Cell Calcium.* 37:283–299.